Journal of Sound and Vibration (2000) **237**(2), 337–355
doi:10.1006/jsvi.2000.3029, available online at http://www.idealibrary.com on IDEAL®

ON THE ACOUSTIC ABSORPTION OF POROUS MATERIALS WITH DIFFERENT SURFACE SHAPES AND PERFORATED PLATES

WEN-HWA CHEN†, FAN-CHING LEE‡ AND DAR-MING CHIANG‡

Department of Power Mechanical Engineering, National Tsing Hua University, Hsinchu, Taiwan 30043, *Republic of China*

(*Received* 12 *July* 1999, *and in final form* 7 *April* 2000)

In architectural acoustic design, perforated plates are often used to protect porous materials from erosion. Although porous materials are usually applied to passive noise control, the effects of their surface shapes are seldom studied. To study the acoustic absorption of porous materials with different surface shapes and perforated plates, an efficient finite element procedure, which is derived by the Galerkin residual method and Helmholtz wave propagation equation, is used in this work. The two-microphone transfer function method and the modified Ingard and Dear impedance tube testing system are employed to measure the parameters deemed necessary for the finite element analysis, such as complex wave propagation constant, characteristic impedance and flow resistivity. For verifying the finite element results, the two-microphone transfer function method is also applied to measure the absorption coefficients of the discussed acoustic absorbers. Four surface shapes of commercially available porous materials, i.e., triangle, semicircle, convex rectangle and plate shapes, are chosen for analysis. The porosity of perforated plates is then evaluated. Finally, the distinct effect of the flow resistivity of porous materials on the acoustic absorption is demonstrated.

1. INTRODUCTION

The porous materials, involving fibrous materials and foams, and perforated plates are widely used in architectural acoustic design owing to their acoustic absorption characteristics, easy arrangement and light weight [1–4]. In general, the porous materials absorb sound well at high-frequency bands while perforated plates work at low-frequency bands. In practical applications, porous materials are always coped with perforated plates for protecting porous materials from erosion. These assemblies would shift the resonance frequency, which is mainly induced by the perforated plate, to low-frequency bands and enhance the acoustic absorption near the resonance frequency. But, the acoustic absorption at high-frequency bands will be reduced. Therefore, how these assemblies influence the acoustic absorption is valuable to be studied orderly and becomes one of the objectives of this work.

In literatures, there are many discussions about acoustic absorbers. For examples, Davern [5] described how the physical elements of perforated plates backed with porous materials and airgap can change the specific acoustic impedance and absorption coefficient

†Professor
‡Graduate Student

0022-460X/00/420337 + 19 $35.00/0

by an experimental procedure. Dunn and Davern [6] and Jinkyo *et al.* [7] discussed the acoustic impedance of multi-layer absorbers and indicated the design concept of multi-layer absorbers. Craggs [8, 9] applied eight-node isoparametric elements to simulate rigid porous absorbers and revealed good agreement with exact solution. However, the surface shape of above acoustic absorbers is limited to plate shape. Recently, Easwaran and Munjal [10] used Galerkin finite element method combining bulk reaction of fibrous absorbers to explore the sound reflection coefficient of wedge fibrous absorbers. Kang and Bolton [11] further discussed the acoustic absorption of porous materials and sound transmission through foam-lined double-panel structures by conventional acoustic finite elements. The results of above two papers have shown that the porous materials with wedge shape would improve the acoustic absorption and transmission loss in some frequency bands.

To examine how surface shapes and sizes of porous materials with perforated plates affect acoustic absorption, a finite element procedure, derived from the Galerkin residual method and Helmholtz wave propagation equation [10], is established in this work. For measuring the parameters of porous materials that are required for finite element analysis, say, complex wave propagation constant, characteristic impedance and flow resistivity, the two-microphone transfer function method [12] and the modified Ingard and Dear impedance tube testing systems [13] are employed. Four surface shapes of commercially available porous materials, i.e., triangle, semicircle, convex rectangle and plate shapes are selected in the analysis. In addition, for verification purpose, the two-microphone impedance tube combining the transfer function method is also applied to measure the absorption coefficient of the acoustic absorbers. Good correlation between the finite element results and the measured data is observed. The acoustic absorption of various surface shapes, size and flow resistivity of porous materials and different porosity of perforated plates is then studied in detail. Those would be of help for the design of acoustic absorbers.

2. FINITE ELEMENT ANALYSIS

Similar to the formulation procedure as used by Easwaran and Munjal [10], the present finite element model is developed as follows. Considering the impedance tube domain as shown in Figure 1, the Helmholtz wave propagation equation can be written as

$$\nabla^2 P_a + k_a^2 P_a = 0 \quad \text{in } \Omega_a \tag{1}$$

and

$$\nabla^2 P_m + k_m^2 P_m = 0 \quad \text{in } \Omega_m, \tag{2}$$

where Ω_a and Ω_m are the domains of air and porous materials respectively. (P_a, P_m) and (k_a, k_m) are the sound pressures and wave numbers in air and porous materials respectively, where $k_a = \omega/c_a$ and $k_m = -\mathrm{i}\gamma$. c_a is the sound speed in air, ω is the angular frequency of excitation and γ is the complex wave propagation constant.

The boundary conditions can be quoted as follows:

(a) For the rigid boundaries say, rigid wall S_{ra} and S_{rm} and boundary of perforated plate S_{rp},

$$\frac{\partial P_a}{\partial n} = 0 \quad \text{on } S_{ra} \text{ and } S_{rp} \tag{3}$$

and

$$\frac{\partial P_m}{\partial n} = 0 \quad \text{on } S_{rm}. \tag{4}$$

(b) For the interface between air and porous materials S_{am},

$$\bar{\mathbf{n}}_a \cdot \bar{\mathbf{u}}_a = -\bar{\mathbf{n}}_m \cdot \bar{\mathbf{u}}_m \tag{5}$$

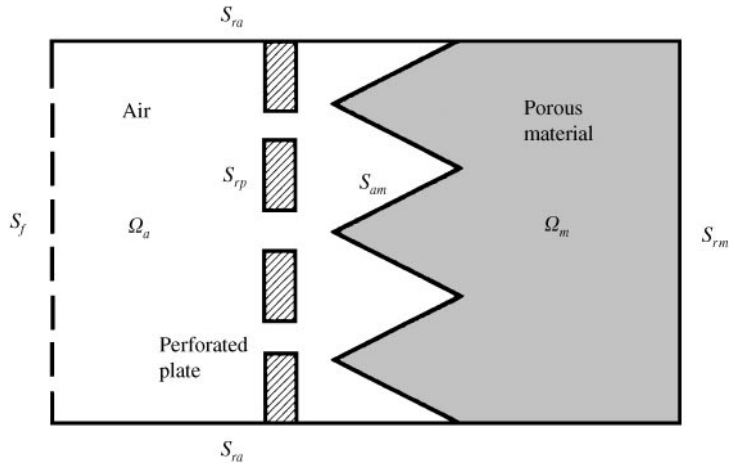

Figure 1. The impedance tube domains.

and

$$\frac{\partial P_j}{\partial_n} = -\mathrm{i}\rho_j \omega \bar{\mathbf{u}}_j \cdot \bar{\mathbf{n}}_j (j = a \text{ or } m), \tag{6}$$

where $P_j (j = a \text{ or } m)$ are the sound pressures of air or porous materials at the interface S_{am}. $\bar{\mathbf{n}}_a$ and $\bar{\mathbf{n}}_m$ are respectively the unit vectors normal to interface S_{am} directed to domains Ω_a and Ω_m. $\bar{\mathbf{u}}_a$ and $\bar{\mathbf{u}}_m$ are the particle velocity vectors of air and porous materials at the interface S_{am} respectively. ρ_a is the density of air and ρ_m is the complex density of porous materials.

(c) For the exciting boundary S_f,

$$\frac{\partial P_a}{\partial_n} = -\mathrm{i}\rho_a \omega u_f, \tag{7}$$

where u_f is the external excitation particle velocity on the boundary S_f.

For the Galerkin finite element analysis, it starts with the governing differential equation. The residual for an approximate trial solution is minimized by weighting functions. A set of shape functions in the domain and on the boundaries has been chosen as the weighting functions. By the first form of Green's theorem in the domains Ω_a and Ω_m, one has (in matrix form)

$$\begin{aligned}
&\sum_{i=1}^{m_a} \int_{\Omega_{ai}} (\nabla\{N\}_a \nabla\{N\}_a^{\mathrm{T}} \{P\}_a - k_a^2 \{N\}_a \{N\}_a^{\mathrm{T}} \{P\}_a)\, \mathrm{d}\Omega_{ai} \\
&\quad + \sum_{i=1}^{m_m} \frac{\rho_a}{\rho_m} \int_{\Omega_{mi}} (\nabla\{N\}_m \nabla\{N\}_m^{\mathrm{T}} \{P\}_m - k_m^2 \{N\}_m \{N\}_m^{\mathrm{T}} \{P\}_m)\, \mathrm{d}\Omega_{mi} \\
&\quad = \sum_{i=1}^{m_f} -i\rho_a \omega \int_{S_{fi}} \{N\}_a u_f \, \mathrm{d}S_i,
\end{aligned} \tag{8}$$

where $\{N\}_a$ and $\{N\}_m$ are the shape functions taken in the domains Ω_a and Ω_m respectively. m_a, m_m and m_f are the element numbers of discretization in the domains Ω_a and Ω_m and on

the boundary S_f respectively. $\{P\}_a$ and $\{P\}_m$ are the nodal sound pressures in the regions $\Omega_a + S_{ra} + S_{rp} + S_f$ and $\Omega_m + S_{rm}$, respectively.

Let

$$[K]_j = \sum_{i=1}^{m_j} \int_{\Omega_{ji}} (\nabla\{N\}_j \nabla\{N\}_j^{\mathrm{T}})\,\mathrm{d}\Omega_{ji} \quad (j = a \text{ or } m), \tag{9}$$

$$[M]_j = \sum_{i=1}^{m_j} \int_{\Omega_{ji}} (\{N\}_j \{N\}_j^{\mathrm{T}})\,\mathrm{d}\Omega_{ji} \quad (j = a \text{ or } m) \tag{10}$$

and

$$\{F\} = \sum_{i=1}^{m_f} -\mathrm{i}\rho_a \omega \int_{s_{fi}} \{N\}_a u_f \,\mathrm{d}S_i. \tag{11}$$

Then, equation (8) can be rearranged as

$$\lfloor [T]_a \ [T]_m \ [T]_c \rfloor \begin{Bmatrix} \{P\}_a \\ \{P\}_m \\ \{P\}_c \end{Bmatrix} = \{F\}, \tag{12}$$

where

$$[T]_a = [K]_a - k_a^2 [M]_a, \tag{13}$$

$$[T]_m = \frac{\rho_a}{\rho_m} ([K]_m - k_m^2 [M]_m), \tag{14}$$

$$[T]_c = \left([K]_a + \frac{\rho_a}{\rho_m} [K]_m \right) - \left(k_a^2 [M]_a + \frac{\rho_a}{\rho_m} \mu_m^2 [M]_m \right), \tag{15}$$

and $\{P\}_c$ is the nodal pressures on the boundary S_{am}. Hence, once the external excitation particle velocity u_f is known, equation (12) can be solved and the nodal sound pressures ($\{P\}_a$, $\{P\}_m$, $\{P\}_c$) are determined. When the external excitation particle velocity u_f is given as 1 m/s, the input impedance $Z_r (= R_r + \mathrm{i}X_r)$ on the exciting boundary S_f can be caluculated by the nodal sound pressures divided by $\rho_a c_a$ [9]. The acoustic absorption coefficient α is therefore related to the input impedance as

$$\alpha = \frac{4R_r}{(R_r + 1)^2 + X_r^2}, \tag{16}$$

where R_r and X_r are the real and imaginary parts of the input impedance Z_r.

3. TWO-MICROPHONE TRANSFER FUNCTION METHOD

As shown in Figure 2, for the plane wave with angular frequency ω moving in an inviscid medium, the sound pressures $p_1(\omega)$ and $p_2(\omega)$ measured by the first and second microphones are [12]

$$p_1(\omega) = A_i(\omega) \mathrm{e}^{\mathrm{i}k_a z_1} + A_r(\omega) \mathrm{e}^{-\mathrm{i}k_a z_1} \tag{17}$$

and

$$p_2(\omega) = A_i(\omega)e^{ik_a z_2} + A_r(\omega)e^{-ik_a z_2}, \tag{18}$$

where $z_1(z_2)$ is the distance between the first (second) microphone and absorber sample. $A_i(\omega)$ and $A_r(\omega)$ are the incident and reflected amplitudes, respectively.

The transfer function $H_{21}(\omega)$ is defined as

$$H_{21}(\omega) = \frac{p_2(\omega)}{p_1(\omega)} = \frac{e^{ik_a z_2} + R(\omega)e^{-ik_a z_2}}{e^{ik_a z_1} + R(\omega)e^{-ik_a z_1}}, \tag{19}$$

where $R(\omega)$ is the complex reflection coefficient. Rewrite above equation as

$$R(\omega) = \frac{A_r(\omega)}{A_i(\omega)} = \frac{H_{21}(\omega) - e^{-ik_a(z_1 - z_2)}}{e^{ik_a(z_1 - z_2)} - H_{21}(\omega)} e^{i2k_a z_1}. \tag{20}$$

The transfer function $H_{21}(\omega)$ in the above equation can be measured by the digital frequency analysis system accurately. For anechoic room wedges, the reflection coefficient $|R(\omega)|$ is often used to represent the effect of acoustic absorption. The reflection coefficient $|R(\omega)|$ and the absorption coefficient α have the following relationship as

$$|R(\omega)| = \sqrt{1 - \alpha}. \tag{21}$$

Utilizing equation (21), one can evaluate the absorption coefficient α.

4. ACOUSTIC PROPERTIES OF POROUS MATERIALS

Assuming that porous materials, such as fibrous materials and foams, are homogeneous, isotropic and porous, Delany and Bazley [14] and Cummings [15] have given an empirical relationship for the flow resistivity σ, complex wave propagation constant γ and non-dimensionalized characteristic impedance Z_m. The relationships are

$$Z_m = [1 + c_1(f\rho_a/\sigma)^{c_2}] - i[c_3(f\rho_a/\sigma)^{c_4}] \tag{22}$$

and

$$\gamma = k_a\{c_5(f\rho_a/\sigma)^{c_6} + i[1 + c_7(f\rho_a/\sigma)^{c_8}]\}, \tag{23}$$

where f is the sound frequency, $c_1, c_2, \ldots, c_8$ are the material parameters of porous materials. In this work, the complex density ρ_m of porous materials that finite element analysis adopted is expressed by the complex wave propagation constant γ and non-dimensionalized characteristic impedance Z_m as following:

$$\rho_m = -i\rho_a c_a Z_m \gamma/\omega. \tag{24}$$

For evaluating the complex wave propagation constant γ and non-dimensionalized characteristic impedance Z_m, a plate shape absorber with thickness t backed with rigid wall is considered. The specific impedance ζ can be expressed as

$$\zeta = Z_m \coth(\gamma t). \tag{25}$$

The relationship between the specific impedance ζ and the complex reflection coefficient $R(\omega)$ is known as

$$\zeta = \frac{1 - R(\omega)}{1 + R(\omega)}. \tag{26}$$

If two pieces of absorbers with different thicknesses t_1 and t_2 are chosen, then

$$\zeta_1 = Z_m \coth(\gamma t_1) \tag{27}$$

and

$$\zeta_2 = Z_m \coth(\gamma t_2). \tag{28}$$

Eliminating Z_m in equations (27) and (28), one obtains [4]

$$\zeta_1 \tanh(\gamma t_1) - \zeta_2 \tanh(\gamma t_2) = 0. \tag{29}$$

For a specific frequency, these ζ_1 and ζ_2 can be measured by the two-microphone impedance tube system. Using the Newton–Raphson method, one can evaluate the complex wave propagation constant γ by equation (29). Then, from equation (27) or equation (28), one can attain the non-dimensionalized characteristic impedance Z_m.

For measuring the flow resistivity σ of porous materials, Ingard and Dear [13] employed the formula

$$\sigma = \frac{\rho_a c_a}{t} 10^{(L_{p1} - L_{p2})/20}, \tag{30}$$

where L_{p1} and L_{p2} are the sound pressure levels measured by the first and second microphones respectively.

The procedure in the experiments for experiments for measuring the specific impedance ζ and flow resistivity σ that above equations involved would be explained below.

5. EXPERIMENTS

The experiments are divided into two parts. One is applying the two-microphone transfer function method to measure the specific impedance ζ and absorption coefficient α. The other is implementing the modified Ingard and Dear impedance tube system to measure the flow resistivity σ of porous materials. Figure 2 and 3 illustrate the instruments used in this work. The above sections have already presented the methods used to evaluate the absorption coefficient α and the specific impedance ζ. By the two-microphone impedance tube system as shown in Figure 2, the complex reflection coefficient $R(\omega)$ can be measured and determined by equation (20). Therefore, the absorption coefficient α and specific impedance ζ can be obtained from equations (21) and (26) respectively. It is noted that when the absorption coefficient α of the absorber is measured at different frequency bands, the upper limited frequency ($f_u < 0{\cdot}586 c_a/d_u$) is of critical concern, where d_u denotes the diameter of the impedance tube. By our instruments, the limitation of measured frequency range is 100–1850 Hz, and the specific impedance ζ and absorption coefficient α are made with an interval of 50 Hz. Besides, according to the limitation described by Chung and Blaser [12], the distance between the first and second microphones must be less than $c_a/2f_u$.

Herein, the flow resistivity σ is defined as $\Delta P/vt$, where ΔP is the air pressure differential across the absorber and v is the particle velocity perpendicular to the surface of the absorber

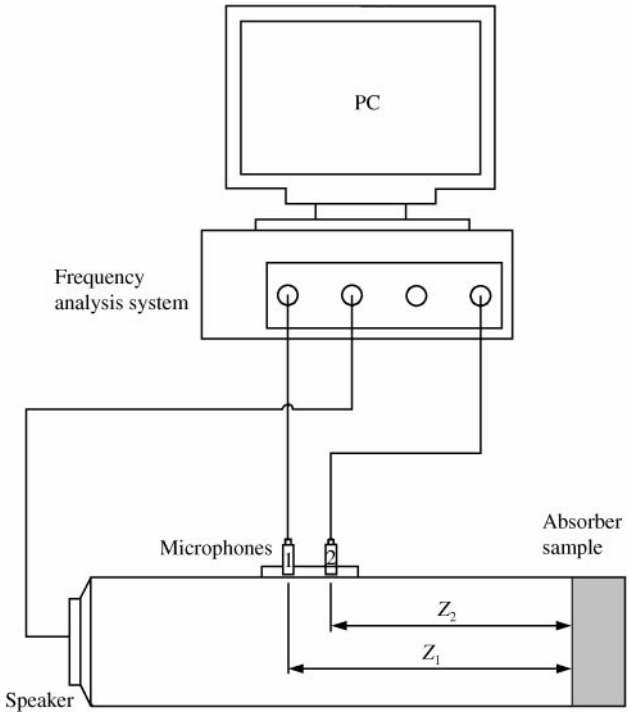

Figure 2. The two-microphone impedance tube system.

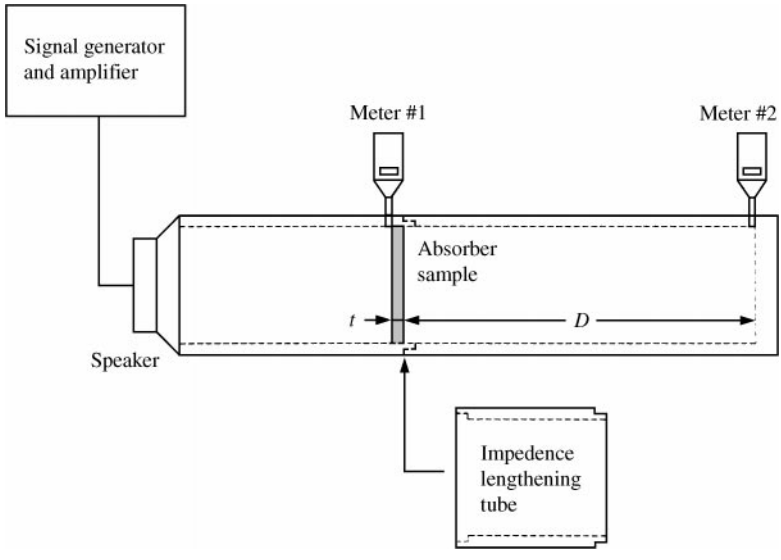

Figure 3. The modified Ingard and Dear impedance tube system.

with thickness t. In this work, the modified Ingard and Dear impedance tube system as shown in Figure 3 is applied to measure the flow resistivity σ. The microphones originally used by Ingard and Dear [13] are replaced by the sound pressure level meters without any weighting for rapidly measuring the sound pressure levels L_{p1} and L_{p2}. The experimental

procedure using the modified Ingard and Dear impedance tube system is summarized as follows:

(1) Place the absorber into the impedance tube as shown in Figure 3. A pure tone with the frequency below 100 Hz is incident to the impedance tube. However, the relationship for the wavelength λ and the distance D between the absorber and the end of the impedance tube must be $D = (2n - 1)\lambda/4$ $(n = 1, 2, \ldots)$.
(2) Record the sound pressure levels L_{p1} and L_{p2} measured by the first and second sound level meters respectively.
(3) Substitute L_{p1} and L_{p2} into equation (30) and evaluate the flow resistivity σ.
(4) Connect the impedance lengthening-tube. Repeat steps (1)–(3) to ensure the flow resistivity σ is a constant at the studied frequency band.

It is noted that the absorber thickness t should be significantly smaller than the wavelength λ of the incident sound to ensure that the sound speed passing through the absorber is a constant, that is, no decay occurs.

6. RESULTS AND DISCUSSIONS

To validate the finite element analysis model, the incident absorption coefficient α of the absorber with plate shape is firstly calculated and compared with the exact solution. Owing to that the input impedance Z_r equals the specific impedance ζ for plate shape absorbers, giving the non-dimensionalized characteristic impedance Z_m, complex wave propagation constant γ and absorber thickness t would allows us to evaluate the absorption coefficient α by equations (16) and (25). Herein, 10 eight-node isoparameteric elements are used. Figure 4

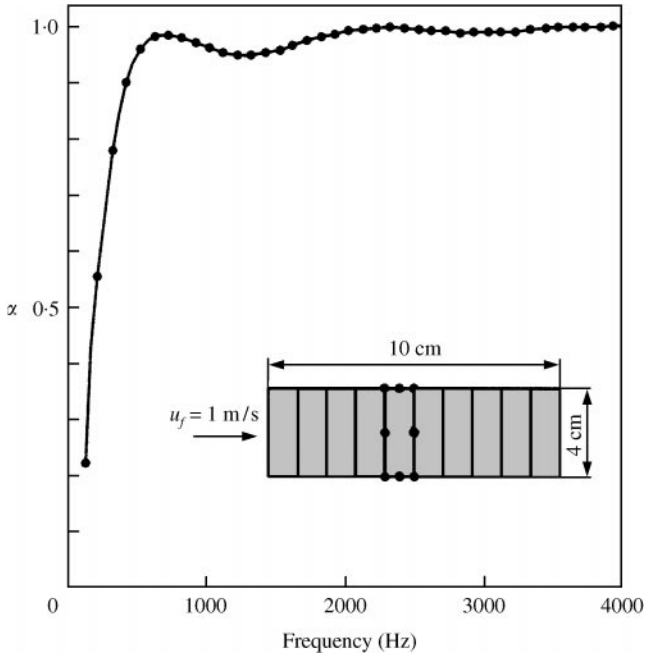

Figure 4. Variation of the absorption coefficient versus frequency: ● ● ●, present (FEM), ——, exact.

depicts the finite element mesh and dimension of the discussed acoustic absorber, where the flow resistivity σ of the absorber is 10,000 N s/m^4. Figure 4 reveals the consonance between the finite element result and exact solution.

Moreover, the model is also used to discuss the reflection coefficient $|R(\omega)|$ of the wedge fibrous absorber which the anechoic room is frequently utilized. Figure 5 illustrates the finite element mesh and dimension of the wedge fibrous absorber, where $s = 1{\cdot}32$ m, $h = 0{\cdot}28$ m, $q = 0{\cdot}2$ m and the flow resistivity $\sigma = 24{,}000$ N s/m^4. Figure 6 reveals the correlation among various methods [10, 16] where Easwaran and Manjal [10] used 432 triangular elements (259 nodes) and present work uses 85 eight-node isoparameteric elements (253 nodes). Comparing these two finite element solutions with experimental data, it reveals that present results are even better when the sound frequency exceeds 150 Hz.

About the numerical simulation of perforated plates, we mesh the air in the hole of the perforated plate and assume the boundary on the perforated plate to be the rigid wall

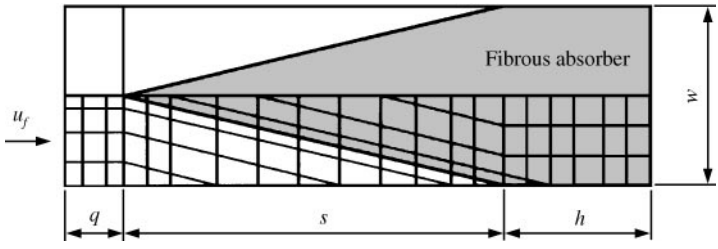

Figure 5. Finite element mesh for wedge fibrous absorber.

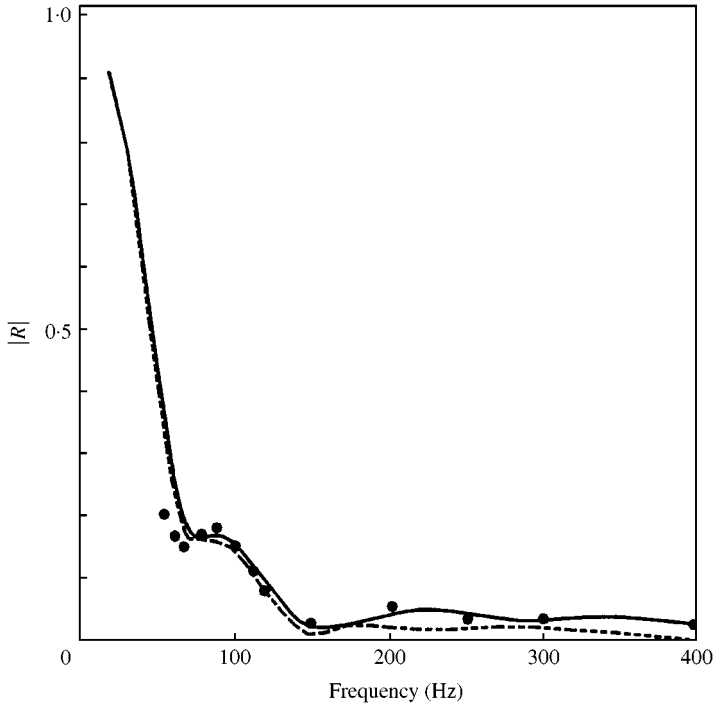

Figure 6. Comparison of the reflection coefficient: • • •, experiment [16]; -----, Easwarn *et al.* [1 0] (FEM); ——, present (FEM).

S_{rp} (see Figure 1). Besides, the hole of the perforated plate considered here is treated as a parallel partition with equivalent porosity b/w in the two-dimensional model as shown in Figure 7. For the validation of this way, the case, which Davern [17] has proposed experimentally, has been chosen. Figure 7 shows the location and dimension of the perforated plate, fibrous absorber and air gap, where the flow resistivity σ of the fibrous absorber is 40,000 N s/m^4. Figure 8 displays the variation of absorption coefficient with frequency for the perforated plate with various porosity. The case without the perforated plate (porosity = 100%) is also presented. The results show that the finite element result would distinctly lower than the experimental data when the perforated plate with lower porosity. This may be attributed to assume the boundary on the perforated plate to be the rigid wall, therefore the acoustic absorption induced by the vibration of the perforated plate is ignored. Besides, the effect of the friction in the hole between the perforated plate and air would also absent according to our assumption, so that the acoustic absorption of total acoustic absorber is abated. However, the entire acoustic absorption tendency of the finite element result is well consisted with the experiment and the difference between the absorption coefficients α of the finite element analysis and experiment is in the reasonable region.

6.1. EFFECTS OF SURFACE SHAPES

The effects of surface shapes of porous materials on acoustic absorption are analyzed by selecting four commercially available surface shapes, i.e. triangle, semicircle, convex rectangle and plate shape. As seen in Figure 9, the total absorber thickness $s + h$ and absorber width w are maintained constant, where h denotes the base thickness and s represents the surface shape thickness. Figure 9 also illustrates the sizes and finite element

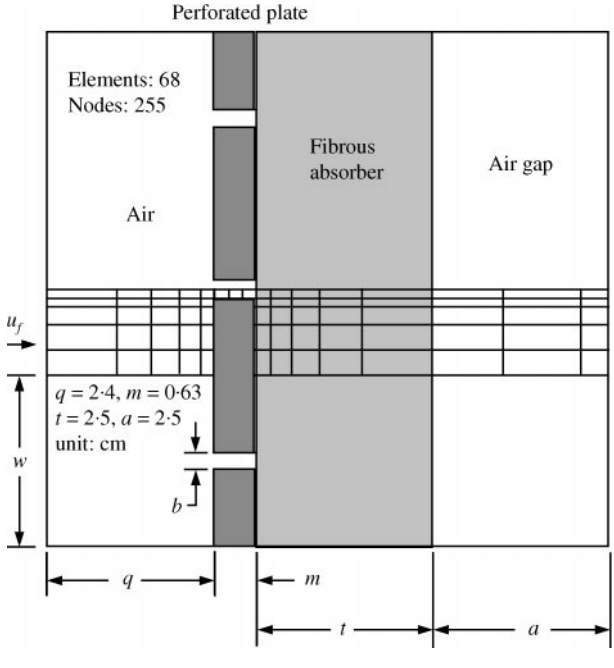

Figure 7. Finite element mesh for perforated plates backed by fibrous absorber and air gap.

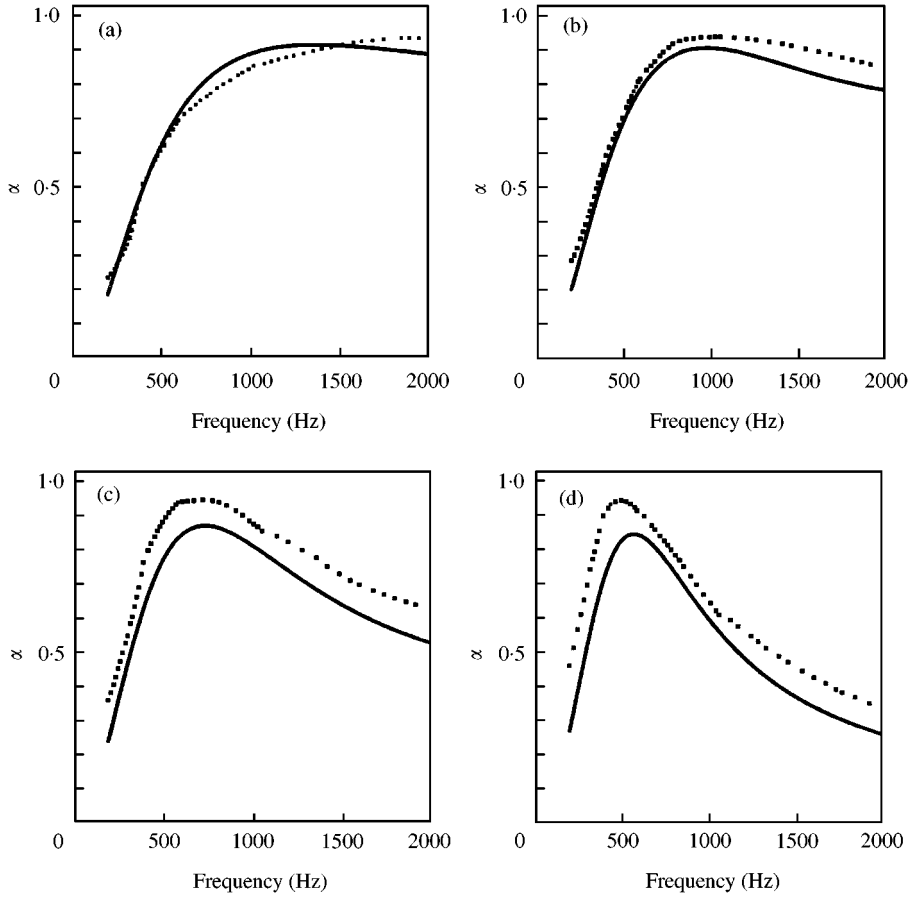

Figure 8. Variation of absorption coefficient with frequency for perforated plates with various porosity: (a) porosity = 100%; (b) porosity = 24%; (c) porosity = 11%; (d) porosity = 4.7%: ●●●, Experiment [17] ——, present (FEM).

meshes of these acoustic absorbers. The thickness chosen here is based on the real thickness of commercially available absorbers. Because the discussed porous materials contain a large amount of symmetrically surface shapes, the top and bottom boundaries on the unit surface shape of acoustic absorber can be treated as the rigid wall boundary S_{rm} (see Figure 1). Therefore, it is sufficient to model a piece of porous materials with different surface shapes by the meshes shown in Figure 9. The acoustic parameters of black foam, say, the flow resistivity σ, the complex wave propagation constant γ and the non-dimensionalized characteristic impedance Z_m can be determined by the experiments as described in sections 4 and 5.

According to Table 1, the flow resistivity σ of black foam which is composed of plastic with porous and open-cell structure is about 10,000 N s/m^4. Its material properties are also listed and compared with those of fibrous material [14] in Table 2. Due to the diameter limitation of the impedance tube adopted in the experiment, only the absorption coefficient α at the frequency band below 1,850 Hz can be measured. Those results are compared with the finite element model in Figure 10. It is found that the finite element model correlates well with the experiment. The reasonable difference between the finite element results and those by the experiment may be attributed to the numerical fittings for the non-dimensionalized

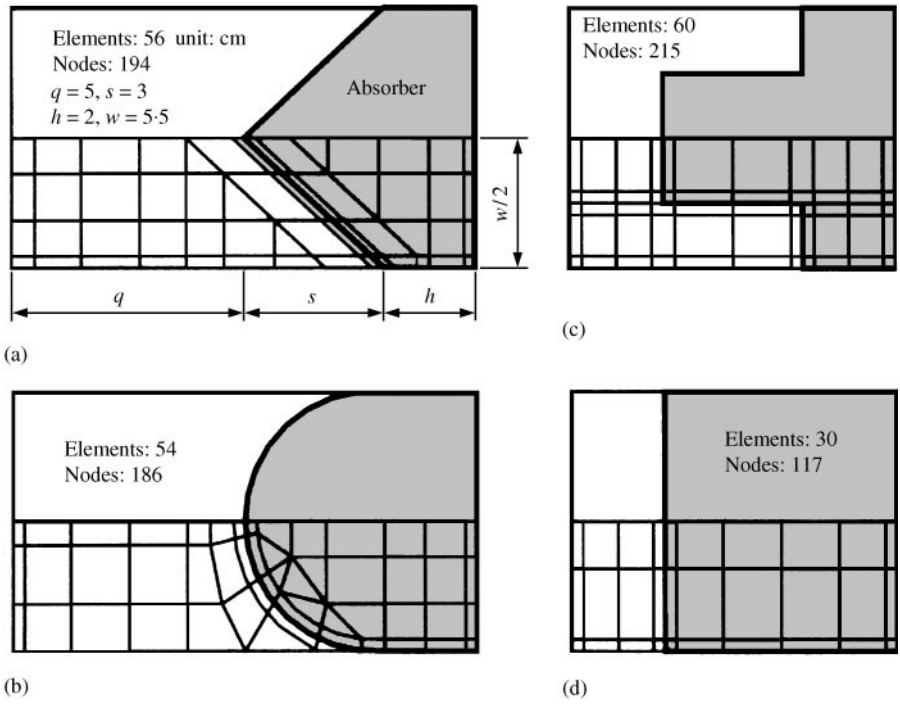

Figure 9. Finite element meshes for different surface shapes of acoustic absorbers: (a) triangle; (b) semicircle; (c) convex rectangle; (d) plate.

TABLE 1

Experimental data for the flow resistivity σ of black foam

	$f = 85{\cdot}75$ Hz $D = 100$ cm			$f = 57{\cdot}17$ Hz $D = 150$ cm		
Thickness t	L_{p1}(dB)	L_{p2}(dB)	σ (N s/m^4)	L_{p1}(dB)	L_{p2}(dB)	σ(N s/m^4)
2·5 cm	96·3	100·5	10,236	94·5	98·4	10,600
1·25 cm	90·3	100·8	9,912	88·5	98·5	10,500

TABLE 2

Material parameters for different porous materials

	c_1	c_2	c_3	c_4	c_5	c_6	c_7	c_8
Black foam (present)	0·271	− 0·381	0·0891	− 0·802	0·163	− 0·681	0·271	− 0·454
Fibrous material [14]	0·0571	− 0·754	0·087	− 0·732	0·189	− 0·595	0·0978	− 0·7

characteristic impedance Z_m and the complex wave propagation constant γ from equations (22) and (23).

Figure 11 summarizes the absorption coefficient α computed by the finite element model for two different acoustic absorbers up to the sound frequency 4,000 Hz. From Figure 11(a),

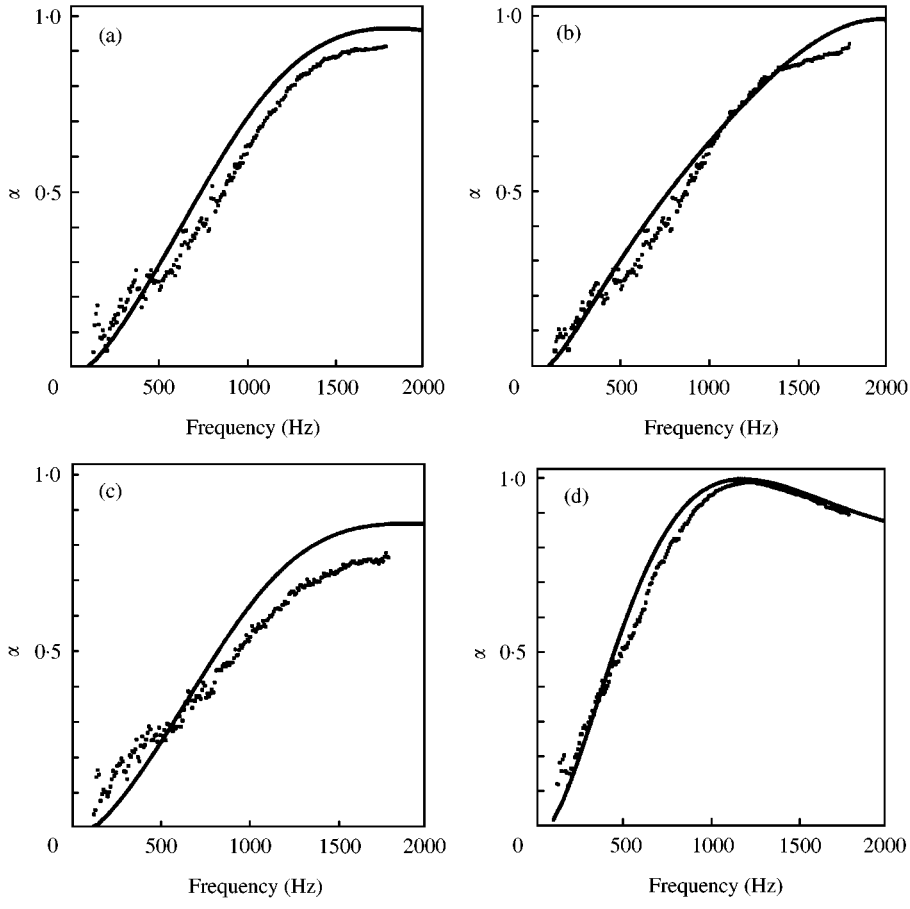

Figure 10. Variation of absorption coefficient versus frequency for different surface shapes of black foam: (a) triangle; (b) semicircle; (c) convex rectangle; (d) plate. ●●●, Experiment (present) ——, FEM (present).

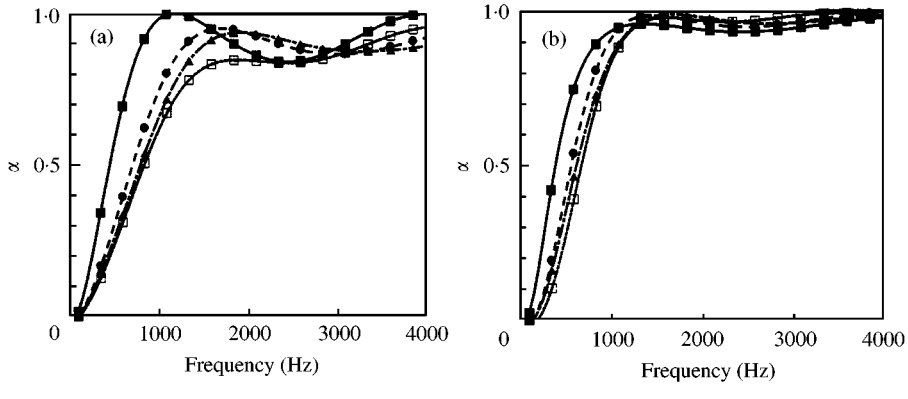

Figure 11. Variation of absorption coefficient versus frequency for different surface shapes and acoustic absorbers: (a) black foam; (b) fibrous material. —■—, Plate; —●—, semicircle; —▲—, triangle; —□—, convex rectangle.

the acoustic absorption of black foam at the frequency band below 1500 Hz is mainly controlled by the quantity of black foam. The higher the quantity which black foam contains implies a better acoustic absorption at this frequency band. However, at the frequency band between 1500 and 3000 Hz, black foam with triangle or semicircle shape would have better acoustic absorption than with other shapes. When the sound frequency is over 3000 Hz, the acoustic absorption of black foam with plate shape is still the best; however, the performance of black foam with convex rectangle shape is in excess of that with triangle or semicircle shape. Figure 11(b) summarizes the absorption effect of various surface shapes for fibrous materials. Figure 11(b) reveals that when the sound frequency is below 1200 Hz, the absorption influence of various shapes resembles Figure 11(a) at the frequency band below 1500 Hz. When the sound frequency is over 1200 Hz, fibrous material with triangle, semicircle or convex rectangle shape has better acoustic absorption than with plate shape. From the above discussions, one can realize that the surface shapes of present porous materials do affect the acoustic absorption distinctly. At some frequency band (for example, over 1200 Hz in Figure 11(b), the effect of surface shapes on the acoustic absorption is even more important than the quantity of absorbers.

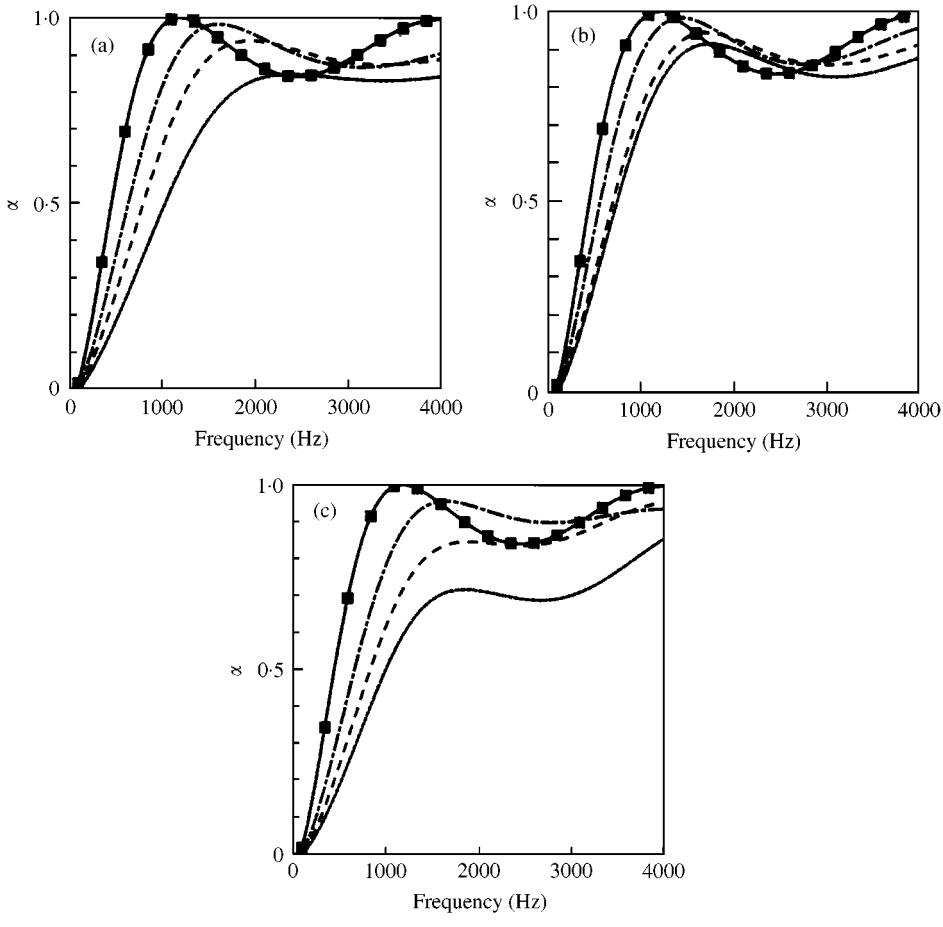

Figure 12. Variation of absorption coefficient versus frequency for different surface shapes and *s*/*h* ratios: (a) triangle; (b) semicircle; (c) convex rectangle. s : h ——, 4 : 1; – – – – –, 3 : 2; —·—·—·, 2 : 3; —■—, plate.

6.2. EFFECT OF ABSORBER SIZE: s/h RATIO

Herein, the s/h ratio, which is defined as the surface shape thickness s divided by the base thickness h is selected to discuss the acoustic absorption of black foam. The total absorber thickness ($s + h$) is maintained 5 cm. For the absorber with plate shape, the s/h ratio is a constant. Figure 12 shows the comparisons of various s/h ratios of black foam with different surface shapes on acoustic absorption. For black foam with triangle shape, when the s/h ratio increases, the curves of the absorption coefficient α versus frequency become plane at the frequency band over 2000 Hz. For black foam with semicircle shape, increasing the s/h ratio causes the reduction of the acoustic absorption at the frequency band below 1500 Hz or over 2500 Hz. An optimum s/h ratio would exist at the frequency band between 1500 and 2500 Hz, where better acoustic absorption is observed as compared with the plate shape. For black foam with convex rectangle shape, increasing the s/h ratio causes a reduction of acoustic absorption at almost all frequency bands. For the case for $s/h = 2/3$ at the frequency band between 1500 and 3000 Hz, the acoustic absorption is again better than that with plate shape. All over the views of these surface shapes, increasing the s/h ratio would approximately cause a reduction of acoustic absorption at the frequency band below

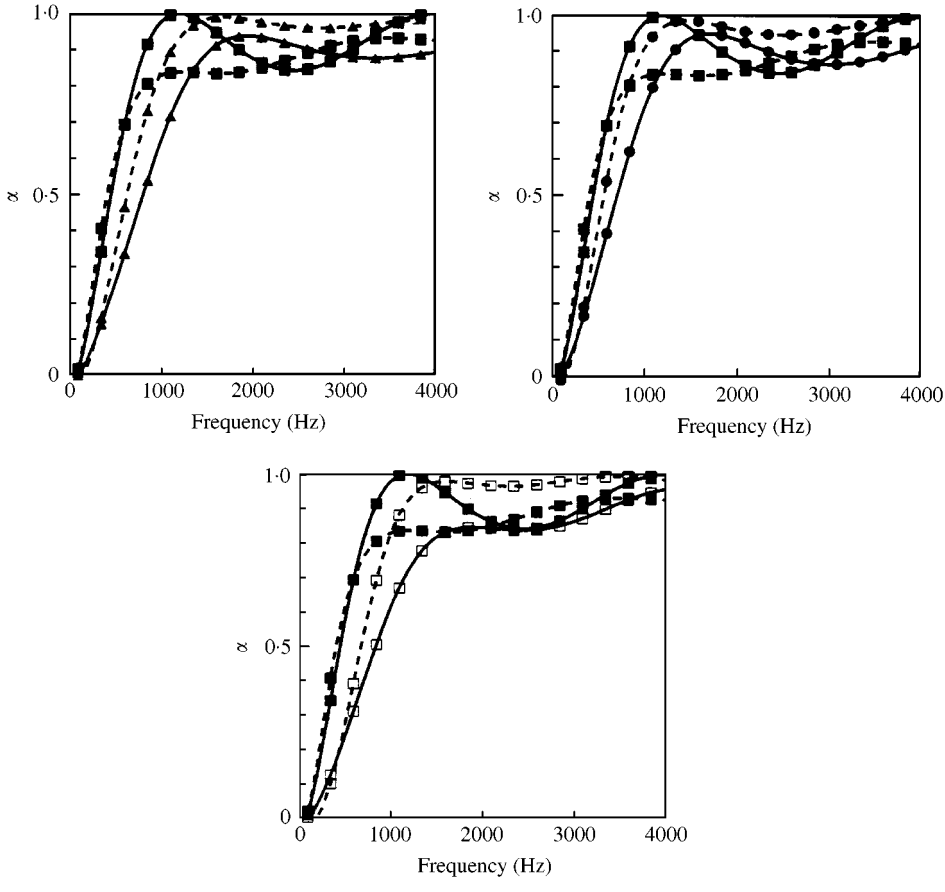

Figure 13. Variation of absorption coefficient versus frequency for different surface shapes and flow resistivity (—— $\sigma = 10\,000$ N s/m^4, -----, $\sigma = 30\,000$ N s/m^4). (a) triangle: —■—, – –■– –, plate; —▲—, – –▲– – triangle. (b) semicircle: —●—, – –●– –, (c) convex rectangle: —□—, – □ –.

1500 Hz or over 3000 Hz. If the s/h ratio decreases, the acoustic absorption would resemble the performance of plate shape absorbers. However, varying the s/h ratio to improve the acoustic absorption would appear at the frequency band between 1500 and 3000 Hz.

6.3. EFFECTS OF FLOW RESISTIVITY σ

The flow resistivity σ of porous materials is an important parameter affecting the acoustic absorption. Generally, increasing the flow resistivity σ of acoustic absorbers with plate shape would enhance and reduce the acoustic absorption at low and high-frequency bands respectively [18]. Therefore, this work would study the effect of increasing the flow resistivity σ of black foam with different surface shapes, where the surface shape thickness $s = 3$ cm and the base thickness $h = 2$ cm. As indicated in Figure 13, increasing the flow resistivity σ of black foam with the plate shape slightly improves the acoustic absorption at the frequency band below 500 Hz, but the acoustic absorption would be inferior at the frequency band over 500 Hz. However, the acoustic absorption of black foams with triangle, semicircle or convex rectangle shape is obviously improved at all frequency bands when the

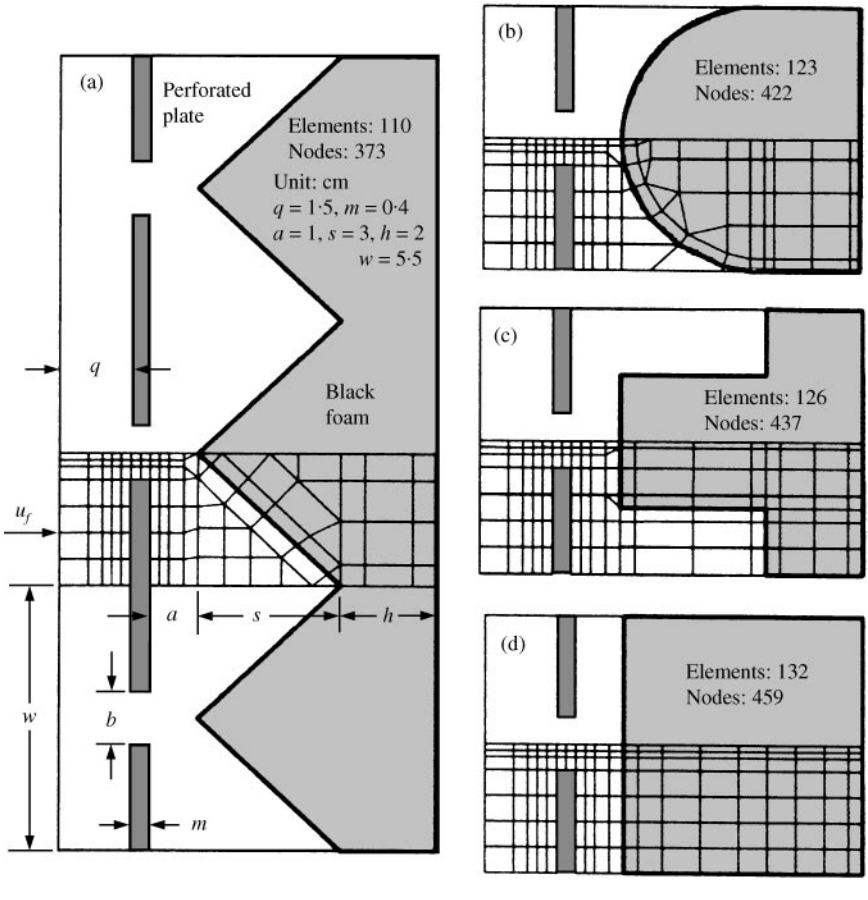

Figure 14. Finite element meshes for perforated plates backed by various surface shapes of black foam: (a) triangle (b) semicircle (c) convex rectangle (d) plate.

flow resistivity σ increases ($\sigma = 30\,000$ N s/m^4). In addition, as $\sigma = 30\,000$ N s/m^4, the acoustic absorption of black foams with triangle, semicircle shape or convex rectangle shape is in excess of the black foam with plate shape at the frequency band over 900 Hz.

6.4. EFFECTS OF POROUS MATERIALS WITH PERFORATED PLATES

For studying the assembly of perforated plates and porous materials on acoustic absorption, four rough surface shapes of commercially available porous materials discussed above and the porosity of perforated plates, say, 100, 20, 10 and 5% are chosen to analyze. The porous material behind the perforated plate is black foam. Figure 14 shows the finite element meshes and sizes for the perforated plate backed with a piece of black foam with various surface shapes. The results shown in Figure 15 indicate that whether the surface shape of black foam behind the perforated plate is, the perforated plate with low porosity (5%) enhances the acoustic absorption at the frequency hand below 700 Hz, but the acoustic absorption would be inferior at the frequency band over 700 Hz.

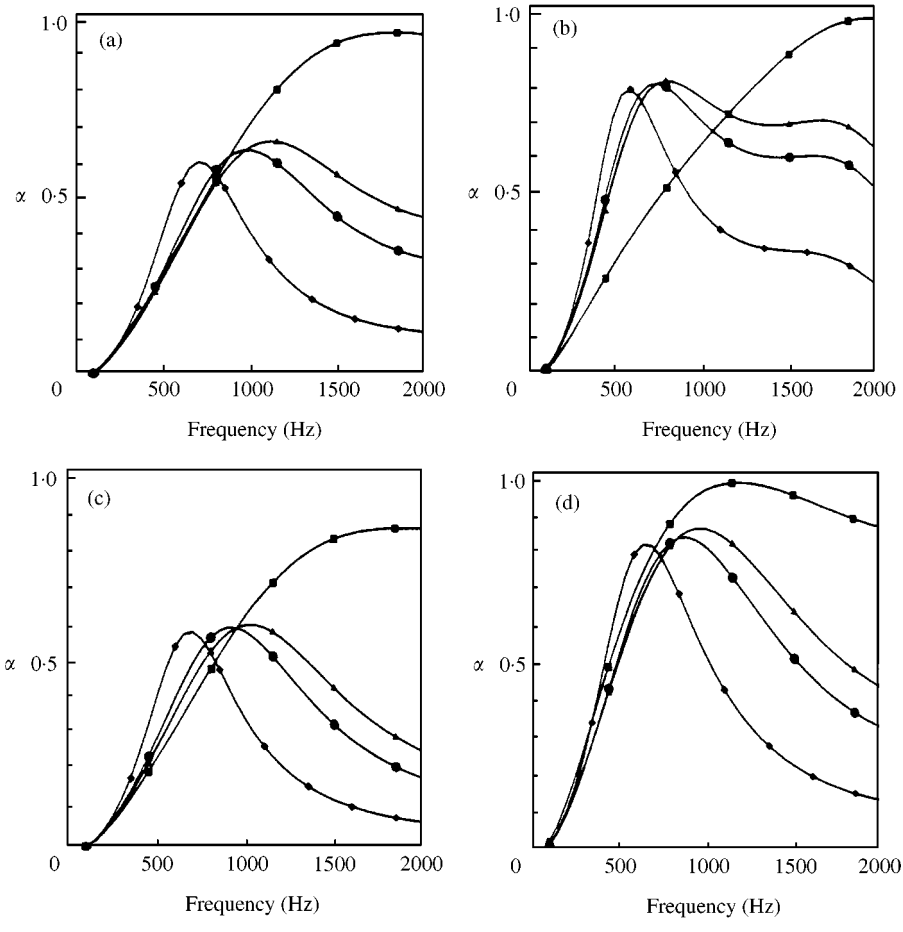

Figure 15. Variation of absorption coefficient with frequency for perforated plates backed by various surface shapes of black foam. (a) triangle; (b) semicircle; (c) convex rectangle; (d) plate. Porosity —■—, 100%; —▲—, 20%; —●—, 10%; —●—, 5%.

All over the views of these assemblies, it approximately reveals that the more material quantities of black foam behind the perforated plate contains, the better acoustic absorption at the acoustic resonance frequency [19] is. Notably, although the material quantities in the triangle shape equal the convex rectangle shape, as seen in Figure 15, the acoustic absorption with triangle shape is better than with convex rectangle shape at the frequency band over the acoustic resonance frequency.

7. CONCLUDING REMARKS

This work elucidates the acoustic absorption of porous materials with different surface shapes and perforated plates. In general, the porous materials containing more material would enhance the acoustic absorption at low-frequency band. For the cases without coping with perforated plates, however, the surface shapes and sizes (s/h ratio) of the porous materials affect the acoustic absorption distinctly at some frequency bands. In addition, except for black foam with plate shape, increasing the flow resistivity σ will improve the acoustic absorption of black foam with different surface shapes at all frequency bands. Finally, the acoustic absorption of perforated plates with different porosity, backed by various surface shapes of black foam, is studied. The results presented in this work can be applied to correctly select the surface shapes of porous materials under different required conditions and would be of help for the design of acoustic absorbers.

ACKNOWLEDGMENT

The partial financial support and experimental assistance from Materials Research Laboratories, Industrial Technology Research Institute, R.O.C., are gratefully acknowledged.

REFERENCES

1. C. ZWIKKER and C. W. KOSTEN 1949 *Sound Absorbing Material*. New York: Elsevier.
2. A. CRAGGS 1977 *Journal of Sound and Vibration* **54**, 285–296. A finite element method for modeling dissipative mufflers with a locally reactive ling.
3. L. E. KINSLER 1982 *Fundamentals of Acoustics*. New York: Wiley-Inerscience.
4. R. J. ASTLEY and A. CUMMINGS 1987 *Journal of Sound and Vibration* **116**, 239–263. A finite element scheme for attenuation in ducts lined with porous material: comparison with experiment.
5. W. A. DAVERN 1977 *Applied Acoustics* **10**, 85–112. Perforated facings backed with porous materials as sound absorbers—an experimental study.
6. I. P. DUNN and W. A. DAVERN 1986 *Applied Acoustics* **19**, 321–334. Calculation of Acoustic Impedance of multi-layer absorbers.
7. L. JINKYO, W. GEORGE and J. SWENSON 1992 *Noise Control Engineering Journal* **38**, 109–117. Compact sound absorbers for low frequencies.
8. A. CRAGGS 1978 *Journal of Sound and Vibration* **61**, 101–111. A finite method for rigid porous absorbing material.
9. A. CRAGGS 1979 *Journal of Sound and Vibration* **66**, 605–613. Coupling of finite element acoustic absorption models.
10. V. EASWARAN and M. L. MUNJAL 1993 *Journal of Sound and Vibration* **160**, 33–350. Finite element analysis of wedges used in anechoic chambers.
11. Y. J. KANG and J. S. BOLTON 1996 *Journal of the Acoustic Society of America* **99**, 2755–2765. Finite element modeling for sound transmission through foam-lined double-panel structures.
12. Y. J. CHUNG and D. A. BLASER 1980 *Journal of the Acoustic Society of America* **68**, 907–913, 914–921. Transfer function method of measuring in-duct acoustic properties. I: theory, II: experiment.

13. K. U. INGARD and T. A. DEAR 1985 *Journal of Sound and Vibration* **103**, 567–572. Measurement of acoustic flow resistance.
14. M. E. DELANY and E. N. BAZLEY 1970 *Applied Acoustics* **3**, 105–116. Acoustic properties of fibrous absorbent material.
15. A. CUMMINGS 1976 *Journal of Sound and Vibration* **49**, 9–35. Sound attenuation in ducts lined on two opposite walls with porous material, with some applications to splitters.
16. W. KOIDAN, G. R. HRUSKA and M. A. PICKETT 1972 *Journal of Sound and Vibration* **52**, 1071–1076. Wedge design for National Bureau of Standards anechoic chambers.
17. W. A. DAVERN 1977 *Applied Acoustics* **10**, 85–112. Perforated facings backed with porous materials as sound absorbers—an experimental study.
18. D. A. BIES and C. H. HANSEN 1980 *Applied Acoustics* **13**, 357–391. Flow resistance information for acoustical design.
19. L. L. BERANEK 1992 *Noise and Vibration Control Engineering*, Chapter 8. New York: Wiley-Interscience.